ELSEVIER

Cardiovascular Research 1 (2000) 000–000

Cardiovascular Research

www.elsevier.com/locate/cardiores
www.elsevier.nl/locate/cardiores

Regional heterogeneity of function in nonischemic dilated cardiomyopathy

Alistair A. Young[a,*], Socrates Dokos[a], Kimerly A. Powell[b], Bernhard Sturm[c], Andrew D. McCulloch[d], Randall C. Starling[b], Patrick M. McCarthy[b], Richard D. White[b]

[a]*Department of Anatomy with Radiology, University of Auckland, Private Bag 92019, 85 Park Road Grafton, Auckland, New Zealand*
[b]*Cleveland Clinic Foundation, Cleveland, OH, USA*
[c]*Ohio State University, Columbus, OH, USA*
[d]*University of California, San Diego, CA, USA*

Received 5 June 2000; accepted 6 October 2000

Abstract

Objective: To quantify regional three-dimensional (3D) motion and myocardial strain using magnetic resonance (MR) tissue tagging in patients with non-ischemic dilated cardiomyopathy (DCM). **Methods:** MR grid tagged images were obtained in multiple short- and long-axis planes in thirteen DCM patients. Regional 3D displacements and strains were calculated with the aid of a finite element model. Five of the patients were also imaged after LV volume reduction by partial left ventriculectomy (PLV), combined with mitral and tricuspid valve repair. **Results:** DCM patients showed consistent, marked regional heterogeneity. Systolic lengthening occurred in the septum in both circumferential ($\%S_C$ $-5\pm7\%$) and longitudinal ($\%S_L$ $-2\pm5\%$) shortening components (negative values indicating lengthening). In contrast, the lateral wall showed relatively normal systolic shortening ($\%S_C$ $12\pm6\%$ and $\%S_L$ $6\pm5\%$, $P<0.001$ lateral vs. septal walls). A geometric estimate of regional stress was correlated with shortening on a regional basis, but could not account for the differences in shortening between regions. In the five patients imaged post-PLV, septal function recovered ($\%S_C$ $9\pm5\%$,$\%S_L$ $6\pm5\%$, $P<0.02$ pre vs. post) with normalization of wall stress, whereas lateral wall shortening was reduced ($\%S_C$ $7\pm6\%$,$\%S_L$ $3\pm3\%$, $P<0.02$ pre vs. post) around the site of surgical resection. **Conclusions:** A consistent pattern of regional heterogeneity of myocardial strain was seen in all patients. Reduced function may be related to increased wall stress, since recovery of septal function is possible after PLV. However, simple geometric stress determinants are not sufficient to explain the functional heterogeneity observed.

Keywords: Cardiomyopathy; NMR; Ventricular function; Heart failure; Computer modeling

1. Introduction

Dilated cardiomyopathy (DCM) of non-ischemic etiology is typically associated with global eccentric left ventricular (LV) hypertrophy, increased LV volume and reduced ejection fraction. Regional heterogeneity of LV function in non-ischemic DCM has been reported using echocardiography [1], tissue Doppler ultrasound [2], left ventriculography [3], cine MRI [4] and radionuclide studies [5]. However, none of these methods allow quantitative measurements of material contraction and deformation. The reported pattern of heterogeneity varies widely between patients, with reduced function noted in inferior, septal and anterior walls and segments of preserved function typically located in the lateral wall [1–5]. The purpose of this study was to quantify the regional variation of three-dimensional (3D) myocardial function in a series of patients with non-ischemic DCM. We hypothesized that there exists a consistent pattern of regional heterogeneity and that this pattern can be characterized using MR tissue tagging.

In order to quantify regional myocardial shortening and deformation (strain), the 3D motions undergone at specific material points must be reconstructed throughout the LV. Myocardial tissue tagging with magnetic resonance (MR) imaging is a non-invasive method in which large numbers

*Corresponding author. Tel.: +1-649-373-599, ext. 6115; fax +1-649-373-7484.
E-mail address: a.young@auckland.ac.nz (A.A. Young).

Time for primary review 32 days.

0008-6363/00/$ – see front matter
PII: S0008-6363(00)00248-0

of material points can be tagged and tracked within the myocardium throughout systole [6,7]. One- and two-dimensional analyses of myocardial function in the image plane have produced useful measurements of regional displacement, torsion and shortening in normal and disease states [8,9]. However, these are dependent on orientation and placement of the tag stripes and image planes, which are typically not in the directions of maximal shortening or lengthening [10,11]. A complete strain analysis requires the estimation of all components of the 3D strain tensor, as well as the associated displacements and rotations. In this investigation we used a finite element model of the LV to reconstruct the 3D displacements of all the tags in all images simultaneously [10]. This method has previously been validated using MR phantoms under well-described deformations [10] and has been applied in vivo to both normal volunteers and patients with hypertrophic cardiomyopathy [11].

2. Methods

All studies were approved by institutional review and ethics committees and all subjects gave informed consent. The investigation conforms with the principles outlined in the Declaration of Helsinki.

2.1. Patient group

Fifteen patients with DCM of non-ischemic origin (confirmed by coronary angiography) were selected for MR imaging from a larger cohort enrolled in a study investigating the role of partial left ventriculectomy (PLV) in end-stage DCM [12]. Patients (Table 1) were selected consecutively on the basis of suitability for MRI (contraindications primarily involved severe shortness of breath, also some patients had implanted pacemakers or defibrillators, or had claustrophobia). All patients were candidates for heart transplant, with NYHA class III (47%) or IV (53%) heart failure and LV end-diastolic diameter = 7 cm by echocardiography [12]. Two patients had inotropic support (Nos. 5 and 9 in Table 1). Five of the patients were also imaged after PLV, in which LV volume was reduced by resection of a portion of the LV free-wall between, and sometimes including, the LV papillary muscles. This procedure also included mitral valve repair involving an annuloplasty ring and an Alfieri repair [12]. Four of the five post-PLV patients also had a tricuspid valve repair, and in one case the papillary muscles were resected and reattached during PLV. In the other ten cases, MR imaging was not possible after PLV due to implanted cardiac defibrillators (ICD), or occasionally a ventricular assist device.

2.2. Image acquisition

All imaging was performed using a 1.5 T Siemens Vision magnet (Siemens Medical Systems, Erlangen, Germany) with a body phase array coil. A segmented 2D Flash sequence was used to acquire breath-hold short-axis and long-axis untagged cine images at end-expiration (end-tidal volume). Nine phase-encoding lines were acquired during each cardiac cycle for each cardiac phase. Echo-sharing techniques were used to double the number of cardiac phase images, giving a temporal resolution of 50 ms. The matrix size of the acquisition was typically 128 × 256 over a FOV of 225–400 mm, resulting in acquisition duration of approximately 14 cardiac cycles. The remaining acquisition parameters were as follows: TR/TE = 100/4.8 ms, flip angle = 20°, slice thickness = 8–10 mm. Velocity compensation was applied in the frequency-encoding direction. End-diastolic volume (EDV), end-systolic volume (ESV), ejection fraction (EF), stroke volume (SV), and myocardial wall mass were calculated from the cine images using commercially available software (Argus, Siemens Medical System, Iselin, NJ, USA) and are shown in Table 1.

A contiguous set of short-axis tagged images of the heart, at levels corresponding to the cine images, was acquired with an echo-shared, segmented k-space version of the Spamm imaging sequence [6]. The tag spacing in the orthogonal grid pattern was 8 mm and the tag lines were oriented at 45° relative to the imaging axes. The imaging parameters were the same as those used for the breath-hold cine MRI acquisition described above, except for TR/TE = 90/4 ms, flip angle = 15°, and lack of velocity compensation in the frequency-encoding direction. A set of four long-axis tagged image slices (temporal resolution 45 ms) were also acquired at equal 45° increments around the LV central axis, starting at the plane passing simultaneously through the mid-septum, center of the LV cavity and LV free-wall. Fig. 1 shows typical short- and long-axis tagged images. Two of the fifteen patients had insufficient long-axis images to perform a 3D analysis, leaving a total of eighteen studies for 3D strain analysis (thirteen baseline and five follow-up studies post-PLV). In four patients the follow-up study was performed 3 months after PLV; the other follow-up study was performed 9 months post-PLV.

2.3. Image processing

The inner and outer boundaries of the LV were manually drawn on all slices at end-diastole (ED) and end-systole (ES) so as to enclose the LV free wall and septum (Fig. 2). Tag stripes were semiautomatically tracked from ED to ES using a previously described and validated technique [10,11]. This resulted in a grid of tracked stripe points with a spacing of approximately 2 mm between points (Fig. 2). The tracked tag points were manually corrected or deleted in cases where the stripe tracking procedure failed due to insufficient image information. The 3D locations of the final stripe points were calculated from the placement of the image slice in space, which was encoded in the image header.

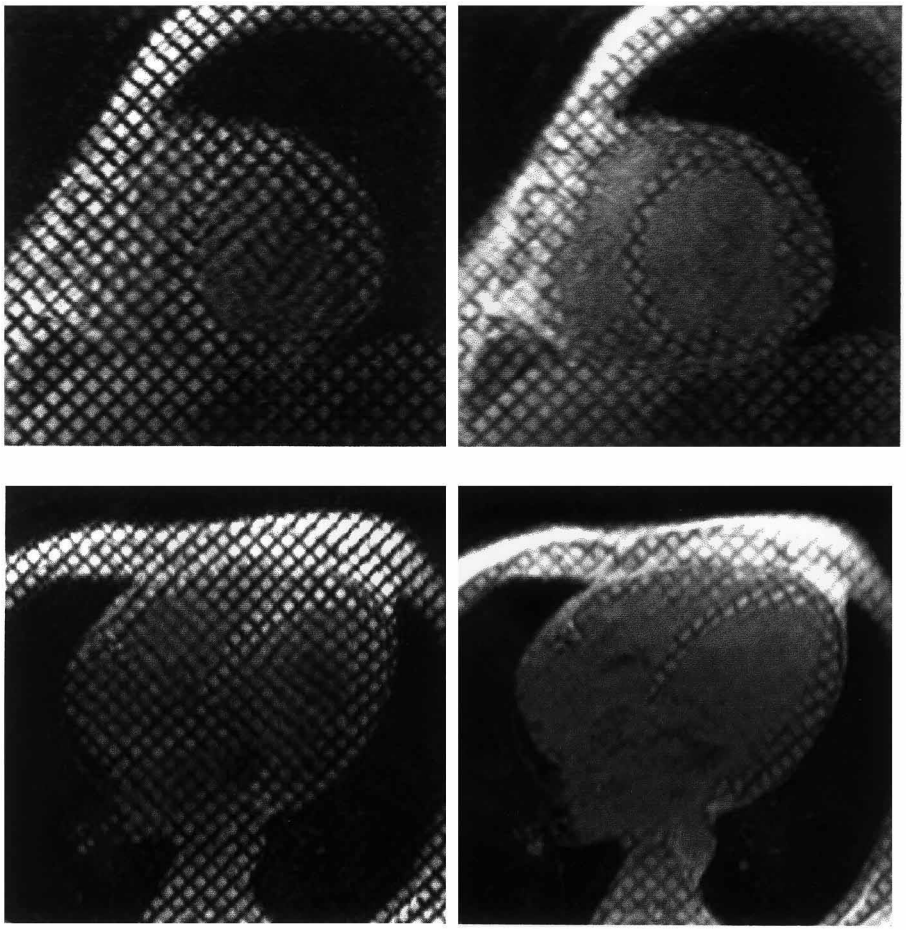

Fig. 1. Typical short (top) and long (bottom) axis tagged images from a DCM patient at ED (left) and ES (right). Note circumferential and longitudinal stretching of the tags in the septal wall during systole.

2.4. Reconstruction of 3D deformation

The geometry and deformation of the LV was reconstructed with the aid of a finite element model, as described previously [10,11]. The model consisted of 16 elements, each with cubic interpolation in the circumferential (C) and longitudinal (L) directions and linear transmural (R) interpolation. Nodal values were shared between neighboring elements to give continuity in both position and slope. The model interpolated the tag displacement constraints between tag and image planes, resulting in a consistent 3D displacement field.

Displacement and strain measures at any point in the model could be calculated using standard methods of continuum mechanics [13,14]. Displacements were separated into three components: longitudinal motion (in the direction of the LV central axis), radial motion (towards or away from the LV central axis) and rotation (about the LV central axis). For these measurements, the LV central axis was defined as the line joining the centroids of the most basal and most apical endocardial short axis contours at each time (ED and ES). The percentage length changes (i.e. the percentage shortening or lengthening of myocardium) was defined in each of the C, L and R directions as

$$\%S_A = \frac{dl_{ED} - dl_{ES}}{dl_{ED}} \cdot 100\% \quad (1)$$

where A is one of the C, L or R directions, $\%S_A$ is the percentage shortening or lengthening in this direction, dl_{ED} and dl_{ES} are the lengths of an infinitesimal material line segment (oriented in this direction at ED) at ED and ES, respectively. Note that lengthening is negative and shortening positive in this description. Shear angles (α_{AB}) were calculated as the change in angle between infinitesimal line segments initially oriented at right angles in the A and B directions, where A and B are any of the C, L or R directions (not both the same). See Appendix for details.

Regional heterogeneity was quantified by calculating the standard deviation of shortening over circumferential or longitudinal regions for each subject (‘regional dispersion’). Regional dispersion was also calculated in 12 normal volunteers from regional data acquired in a previous study using similar methods [11].

2.5. Geometric stress estimate

A geometrically-based estimate of regional stress (GS) was calculated from the model geometry and cuff blood

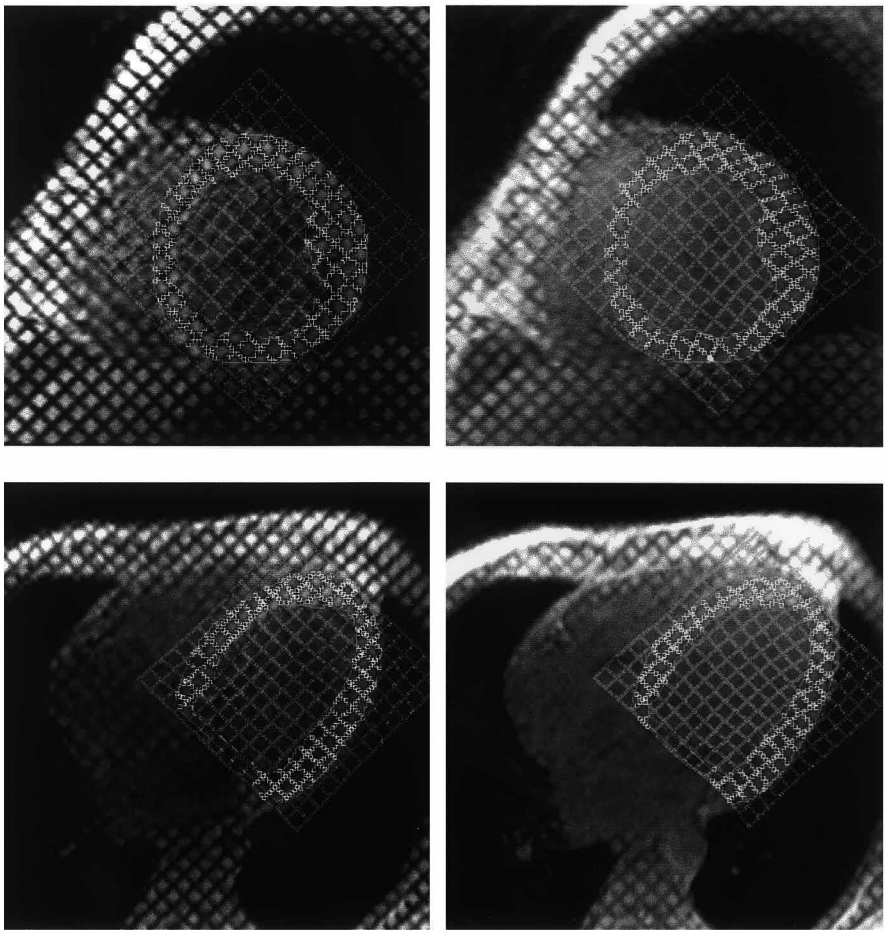

Fig. 2. LV boundaries and tracked stripes shown as an overlay on the same images as Fig. 1.

pressure measurements using Mirsky's thick-walled ellipsoid formula [15]

$$GS = \frac{Pr_{ES}}{t_{ES}}\left(1 - \frac{t_{ES}}{2r_{ES}} - \frac{r_{ES}^2}{2a^2} + \frac{t_{ES}}{8a^2}\right) \quad (2)$$

where $P = (SBP - DSP)/3 + DBP$ is an estimate of mean arterial pressure taken from the systolic (SBP) and diastolic (DSP) cuff pressures, r_{ES} is the regional radius of circumferential curvature at ES, t_{ES} is the regional wall thickness at ES and a is the distance from the origin to the apex (also at ES). Regional circumferential radius of curvature was substituted for the minor semi-axis distance in Eq. (2) in order to provide a regional stress estimate. Curvature was calculated at the model midwall surface using standard formulae of differential geometry, as described previously [16] (a large number of evenly distributed samples were averaged for each region). Longitudinal curvature was not substituted for major semi-axis (a in Eq. (2)), since relatively few long axis slices were available and estimates of longitudinal curvature were found to be variable (longitudinal radii of curvature were often very large and sometimes changed sign around the ventricle). If the term in brackets is ignored, Eq. (2) becomes a simple LaPlacian estimate of stress based on a thin-walled cylinder.

2.6. Statistical analysis

Displacement and strain data were averaged into 16 regions in accordance with the recommendations of the American Society of Echocardiography Committee on Standards [20]. The LV was divided into three longitudinal portions (apex, mid and base) which in turn were divided into four (for the apex) or six (for midventricle and base) regions. Repeated measures ANOVA was used to test for regional differences in displacement and strain as well as changes post-PLV. Global volume and haemodynamic data were compared pre- and post-PLV with a paired t-test. A P value of less than 0.05 was required to reject the null hypothesis that there were no regional differences, or no difference pre- and post-PLV. The patient results were also compared with published data from a set of twelve normal volunteers who were studied previously using a similar 3D tagging analysis [11].

Table 1
Patient data and global function derived from untagged MR images[a]

Patient no.	Age	Sex	Wt, (kg)	Ht, (cm)	EDV (ml)	ESV (ml)	SV (ml)	EF (%)	Mass (g)	SBP (mmHg)	DPB (mmHg)	HR (bpm)
1	57	M	66	168	337	295	42	12	345	97	74	93
2	50	M	93	178	536	435	101	19	437	106	67	103
3	58	M	79	178	737	676	61	8	555	92	64	102
4	68	F	65	167	237	189	48	20	284	117	61	90
5	34	M	86	189	621	567	54	9	453	99	75	118
6	62	M	74	174	327	236	91	28	377	127	79	64
7	67	M	75	193	610	561	49	8	377	80	54	110
8	53	F	65	164	466	408	58	12	374	97	71	88
9	66	M	90	176	292	250	42	14	281	101	70	115
10	47	M	96	166	315	277	38	12	339	126	98	110
11	52	M	87	172	613	545	68	11	614	94	69	99
12	50	F	91	166	184	124	60	33	378	108	68	96
13	63	M	90	177	366	273	93	25	468	127	85	81
Mean	56		81	174	434	372	62	16	406	106	72	98

[a] Ht, height; Wt., weight; EDV, end-diastolic volume; ESV, end-systolic volume; SV, stroke volume; EF, ejection fraction; HR, heart rate; SBP, systolic blood pressure; DBP, diastolic blood pressure. Of the fifteen patients imaged, two had insufficient long axis images for 3D quantification and were therefore not included in the analysis.

3. Results

Global functional parameters measured from the cine (untagged) MR images are shown in Table 1. The average root mean square error between the tracked stripe points and the reconstructed model points was 1.1 mm (range 0.5–1.8 mm) over the thirteen patients, with an average of 5339 stripe points fitted per study. These errors were comparable to the average image pixel size of 1.3 mm. Displacement and strain results are presented in Tables 2 and 3, respectively, in which average values and standard deviations are given for each region.

Table 2
Regional 3D displacement between ED and ES

Region	Rotation[a] (°)	Longitudinal[a] (mm)	Radial[a] (mm)
Apex			
S	−2±5	2.9±1.6	1.0±1.2
P	1±5	−0.2±1.4	1.3±0.9
L	−1±6	−1.2±3.2	2.0±1.3
A	−4±6	0.2±2.7	1.6±1.2
Mid			
AS	−3±3	5.0±3.0	−0.5±2.2
PS	−2±4	4.9±3.6	0.0±1.8
P	0±4	1.5±1.7	1.9±1.2
PL	1±4	0.1±2.6	2.6±1.1
AL	−4±4	0.7±3.1	3.2±1.3
A	−5±3	2.5±1.8	1.4±1.1
Base			
AS	−4±3	3.6±2.1	−0.2±1.4
PS	−3±3	4.2±2.6	0.2±1.7
P	0±2	2.6±2.4	2.7±1.1
PL	0±2	2.5±2.7	2.9±1.2
AL	−6±3	3.3±2.8	2.9±1.1
A	−7±4	3.5±2.8	2.4±1.2

[a] Mean±S.D., $n=13$.

3.1. Displacement

Rotation about the central axis was small and negative (i.e. clockwise as viewed from the apex) in most regions. There was significant regional variation (ANOVA $P<0.001$) with greater rotation in the anterior wall than posterior ($P<0.001$). LV torsion (i.e. the rotation of the apex relative to the base) was also small. This pattern of rotation is very different from the normal anticlockwise rotation of the apex ($+13°$) and clockwise rotation of the base ($-2°$) found in healthy volunteers [11]. Longitudinal displacements (defined as motion parallel to the LV central axis, positive towards the apex) were also smaller than normal (base displacement 3.5 mm vs. 12.5 mm in normal volunteers [11]). Radial displacement is normally inward (i.e. positive) but was reduced in the septum relative to lateral wall (ANOVA $P<0.001$ for overall variation; $P<0.001$ septal vs. lateral), with many patients showing outward septal motion (toward the RV).

3.2. Strain

Circumferential shortening ($\%S_C$ in Table 3) typically ranges from 17 to 21% in the healthy ventricle [11], consistent with shortening of the circumferential muscle fibers. However, there was substantial regional variation in the DCM group (ANOVA $P<0.001$), with circumferential lengthening in the septum in ten patients and minimal $\%S_C$ in the other three. Averaged over midventricle and base regions, septal $\%S_C$ was significantly reduced compared to the lateral wall (-5 ± 7 vs. $12\pm6\%$, $P<0.001$).

Longitudinal shortening ($\%S_L$ in Table 3) also showed significant regional heterogeneity (ANOVA $P<0.001$) with a similar pattern to $\%S_C$, i.e. lengthening in the septum and shortening in the lateral wall (-2 ± 5 vs. $6\pm5\%$, $P<$

Table 3
Regional 3D strain between ED and ES[a]

Region	$\%S_C$	$\%S_L$	$\%S_R$	α_{CL} (°)	α_{CR} (°)	α_{LR} (°)
Apex						
S	−1±7	1±4	0±7	−1±3	−1±5	−3±3
P	3±4	4±4	4±7	−3±2	−2±4	1±4
L	10±7	6±5	0±6	0±4	−2±3	−2±3
A	5±4	3±4	−1±5	−1±4	−1±7	−6±4
Mid						
AS	−6±9	−4±6	3±8	3±4	1±6	−3±4
PS	−4±5	−1±5	3±8	1±4	0±4	−3±4
P	−1±5	1±4	5±5	1±7	−3±4	1±4
PL	10±6	5±4	1±4	4±5	−4±4	3±6
AL	12±6	7±4	−3±6	3±6	1±4	−2±3
A	0±4	0±2	−2±8	0±6	3±7	−3±5
Base						
AS	−5±5	−3±5	2±5	0±3	0±7	1±4
PS	−4±8	−1±4	2±7	1±3	2±3	0±4
P	1±6	5±6	3±6	3±6	1±5	3±3
PL	12±6	7±6	−5±8	4±7	−1±5	4±6
AL	12±5	6±7	−5±7	5±5	2±5	1±4
A	1±3	1±6	2±8	0±5	3±6	1±4

[a] Values are mean±S.D., $n=13$.

0.001). In contrast, typical normal values for $\%S_L$ are relatively homogeneous (ranging from 13 to 18%) [11]. Regional differences in $\%S_C$ and $\%S_L$ between septal and lateral walls are summarized in Fig. 3.

Radial strains ($\%S_R$) were positive in the septal and posterior walls (indicating radial thinning) with wall thickening (reduced in magnitude from normal) in the lateral and anterior walls (ANOVA $P<0.001$). Transverse shears also showed considerable regional heterogeneity (ANOVA $P<0.001$). These were similar in magnitude to normal volunteers; however, α_{CL} is normally positive at the apex [11].

The principal strains (see Appendix) in each region were also calculated but the directions of maximum shortening and lengthening changed markedly from region to region. For example, the maximum shortening in the septum acted in the radial direction but was circumferentially oriented in the lateral wall.

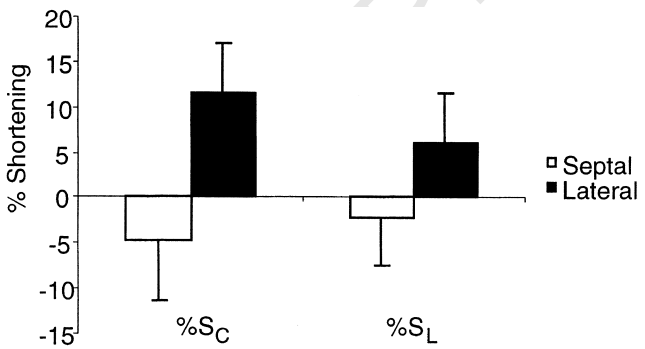

Fig. 3. Circumferential and longitudinal strain expressed as % shortening (+ve) or lengthening (−ve) for septal and lateral walls of the LV (averaged over mid and base levels).

3.3. Geometric stress estimate

Although there was significant regional variation in GS (ANOVA $P<0.001$), this was largely due to the difference in radius of curvature between apex, mid and base levels. The septal wall tended to have greater GS than the lateral wall but the size of this effect was small and reached significance only at the basal level ($P=0.035$). Fig. 4 shows circumferential shortening plotted against circumferential GS at ES for the septal, posterior, lateral and anterior regions averaged at mid and base levels. Separate regressions in each region resulted in a significant correlation between shortening and GS in the lateral ($P<0.003$) and anterior ($P<0.03$) walls. It can be seen that, although there is a relationship between GS and $\%S_C$ in some regions, GS does not explain the regional differences in shortening. A multiple linear regression model (shortening = constant + subject + region + GS + region·GS) was tested with region as a categorical variable and GS as a continuous variable. This resulted in significant effects due to region ($P<0.001$), GS ($P<0.01$) and the interaction between region and GS ($P<0.02$). Similar results were also obtained using a simple LaPlacian stress estimate based on a thin walled cylinder (i.e. ignoring the term in brackets in eqn 2). Thus, the effect due to region on $\%S_C$ is still present after correction for GS, with the relationship between GS and $\%S_C$ also effected by region.

3.4. Post-PLV studies

Table 4 shows a summary of hemodynamic data for the five patients studied after PLV. Average root mean squared error for the finite element model fits was 0.8 mm in the 5

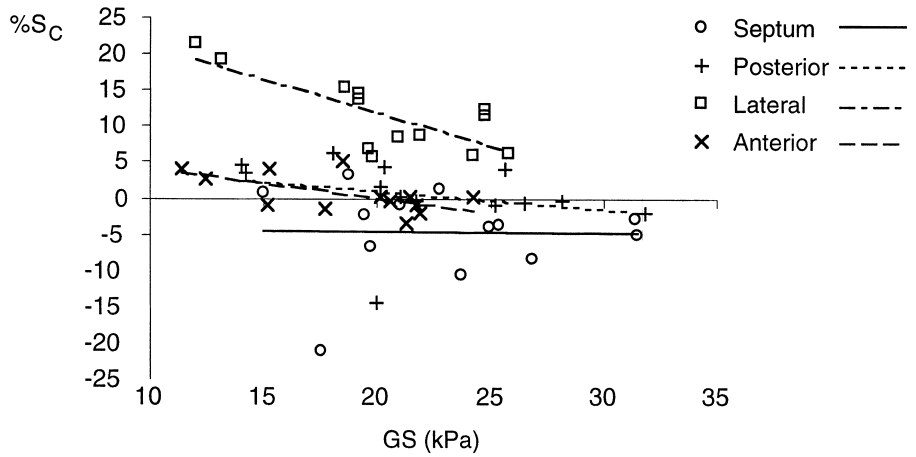

Fig. 4. Regional circumferential shortening (%S_C) vs. regional circumferential wall stress (GS, kPa) for septal, posterior, anterior and lateral regions averaged over mid and base levels ($n=13$).

post-PLV studies (range 0.7–1.1 mm) with an average of 4305 points fitted per study. Rotation was reduced in magnitude post-PLV ($-5\pm5°$ pre vs. $-2\pm3°$ post, $P<0.001$) and the radial displacement of the septum changed from towards the RV (-1.4 ± 0.9 mm pre) to towards the LV (3.3 ± 0.7 mm post, $P<0.01$ pre vs. post).

Circumferential strain in the septum after PLV had recovered to more normal shortening values ($9\pm5\%$ on average, $P<0.02$ pre vs. post). Circumferential shortening was also increased in the anterior wall at all levels ($11\pm3\%$ on average, $P<0.01$ pre vs. post). In contrast, function in the lateral portion of the LV free-wall was reduced (7 ± 6, $P<0.02$ pre vs. post). This was due to the formation of scar tissue at the site of the surgical resection. %S_L also showed a recovery in septal shortening post ($6\pm5\%$, $P<0.02$) and a reduction in lateral wall shortening at all levels ($3\pm3\%$, $P<0.01$).

Fig. 5 shows a plot of regional circumferential shortening in the 5 patients studied pre- and post-PLV, together with regional GS. GS was reduced in all regions (pre vs. post) due to the reduction in midwall radius of curvature. Typical normal values of mean blood pressure (80 mmHg), ES midwall circumferential radius of curvature (24 mm), ES wall thickness (13 mm) and semi-major axis (55 mm) result in a GS of 12.4 kPa. Since normal circumferential shortening is typically 19% [11], this gives a point marked * in Fig. 5. Shortening in the septal, anterior and posterior wall thus moved toward more normal values with GS normalization; however, lateral walls moved toward lower shortening values, consistent with loss of contractility at the site of surgical resection.

3.5. Regional dispersion

The dispersion of regional circumferential and longitudinal shortening is compared between DCM patients, historical normal volunteers and post-PLV studies in Table 5. Circumferential dispersion was defined as the standard deviation of regional shortening between circumferential regions at each of the apex, midventricle and base levels, whereas longitudinal dispersion was defined as the standard deviation of shortening between longitudinal regions at each of the septal, posterior, lateral and anterior sites. Circumferential dispersion in both %S_C and %S_L was markedly greater in the DCM group than in normal volunteers ($P<0.01$), and was reduced overall in the five patients imaged after PLV (ANOVA $P<0.05$). Circumferential dispersion in %S_C remained higher than normal after PLV ($P<0.01$). There were no differences in longitudinal dispersion of shortening between groups.

Table 4
Patient global function for post-PLV studies derived from untagged MR images[a]

Patient	EDV (ml)	ESV (ml)	SV (ml)	EF (%)	Mass (g)	HR (bpm)	SPB (mmHg)	DBP (mmHg)
1	170	121	49	29	236	81	114	75
2	272	196	76	28	297	91	89	59
3	311	223	89	29	365	69	104	62
4	216	131	85	39	233	58	123	56
5	404	314	90	22	313	91	114	68
Mean	274.6*	196.8*	77.8	29.4*	288.8*	78.0*	108.8	64.0

[a] Headings as for Table 2. *, $P<0.05$ pre vs. post. Patient numbers 1–5 correspond to Table 1.

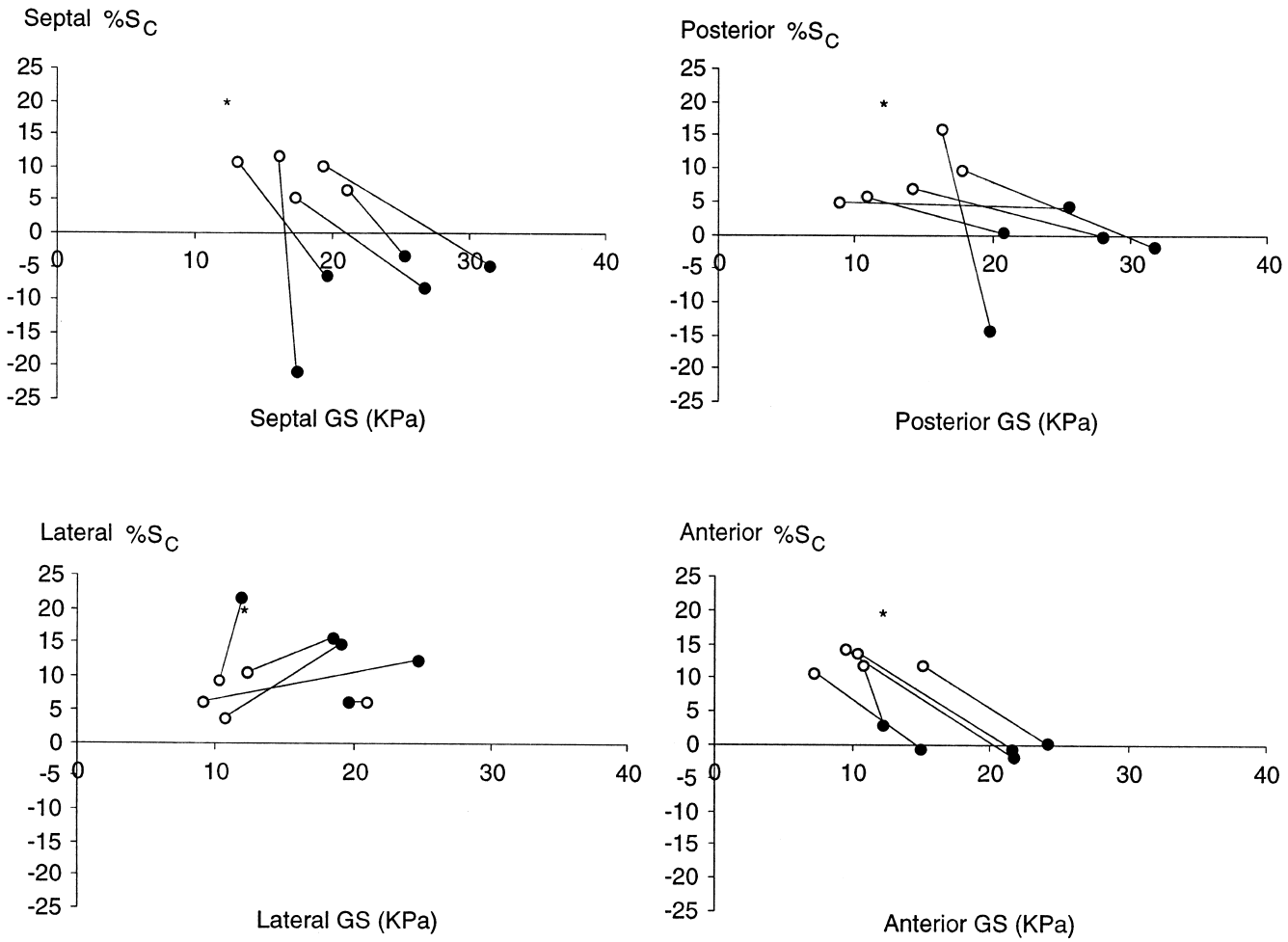

506

507 Fig. 5. Circumferential shortening (%) vs. regional circumferential wall stress (kPa) for the five patients pre (solid circles) and post (open circles) PLV. For
508 reference, * denotes typical normal values.

526 ## 4. Discussion

527 ### *4.1. Regional heterogeneity of function*

528 Regional heterogeneity in normal LV shortening has
529 been previously quantified using a variety of techniques
530 [11,21–24]. In a MR tagging study of hypertrophic
531 cardiomyoapthy (HCM), normal $\%S_C$ ranged from 17 to
532 21% and was generally greater in the lateral and anterior
533 walls than the septum or posterior walls [11], while $\%S_L$
534 ranged from 14 to 20% and was diminished at the basal
535 septum relative to posterior and lateral walls. Septal
536 shortening was further reduced in HCM patients. Similar
537 regional variations were also seen in human transplant
538 recipients using radiopaque markers [21] and in dogs using
539 ultrasonic crystals [22]. Van Rugge et al. [23] found that

509 Table 5
510 Circumferential and longitudinal dispersion in $\%S_C$ and $\%S_L$ in DCM patients and historical normal volunteers [11]
511
512
513
514
515

		Circumferential dispersion			Longitudinal dispersion			
		Apex	Mid	Base	Septum	Posterior	Lateral	Anterior
516 $\%S_C$	DCM	5.8±3.2	8.0±4.7	8.1±4.4	3.1±1.9	3.2±2.1	2.5±1.6	3.6±1.7
517	Post-PLV	4.7±1.3	5.2±1.4	5.1±1.3	2.6±1.3	3.5±2.0	2.9±1.7	2.6±2.3
518	Normal	3.6±1.7*	2.4±1.1†,‡	2.9±0.7†,‡	2.3±1.3	3.3±2.8	1.7±1.2	2.9±1.1
519 $\%S_L$	DCM	3.7±1.9	4.9±2.4	6.0±2.6	3.3±1.7	4.1±1.9	3.4±2.2	3.3±2.1
520	Post-PLV	3.7±1.9	2.7±0.8‡	4.2±2.1	2.2±1.7	5.4±2.5	2.1±0.6	2.8±0.1
521	Normal	3.6±1.7	2.4±1.1*	2.9±0.7*	2.6±1.3	3.3±2.8	1.7±1.2	2.9±1.1

522
523 *, $P<0.05$ DCM vs. normal volunteers.
524 †, $P<0.001$ DCM vs. normal volunteers.
525 ‡, $P<0.001$ DCM post-PLV vs. normal volunteers.

regional wall thickening was highest in the posterolateral wall and lowest in the septal wall at both baseline and during peak dobutamine infusion in 23 normal volunteers using MR cine imaging. A similar study using 2D echocardiography found that heterogeneity in wall thickening could be enhanced by dobutamine infusion, with decreased wall thickening in the inferior wall [24]. All these reports show a normal variation in regional shortening which is substantially less than that found in the present study of non-ischemic DCM patients. All DCM patients showed considerable circumferential heterogeneity, particularly at the midventricular and basal levels, with a consistent pattern of septal dysfunction and relatively normal lateral wall function.

Heterogeneity of regional LV function has frequently been noted in patients with non-ischemic DCM [1–5,25]; however, the site of the most severe dysfunction has appeared to vary widely. Many studies have used the coefficient of variation (ratio of standard deviation to the mean value) to quantify variability [1,3]; however, this measure will decrease with increasing mean shortening and may bias comparisons of heterogeneity between DCM and normal subjects. Uematsu et al. [2] measured peak myocardial velocity gradients by tissue Doppler imaging in patients with DCM and found lower velocity gradients in anteroseptal segments than posterior segments. Hayashida et al. [3] noted considerable regional variation using left ventriculography in the right anterior oblique view; however, no consistent patterns were observed and the septum was not well visualized. Sunnerhagen et al. [25] found abnormal wall motion in the apical and anteroapical regions using time–intensity curves from digitized right anterior oblique left ventriculograms. Bach et al. [1] found regional short-axis chord shortening by 2D echocardiography was more frequently preserved in the proximal lateral wall, consistent with the results of the present study. Using ciné MRI, Fujita et al. [4] observed that the normal base–apex gradient of regional ejection fraction was exaggerated in DCM so that the relative loss of function was more severe near the base. However, circumferential variation of function was not quantified. MacGowan et al. [26] used MR tagging to quantify epicardial and endocardial fiber and cross-fiber shortening in nine idiopathic DCM patients. Fiber shortening was reduced in both regions in the DCM patients (8 vs. 15% for epicardium and 9 vs. 18% for endocardium) while cross-fiber shortening was only reduced in the endocardium (16 vs. 31%). Unfortunately, circumferential variation was not reported.

Nonhomogeneous systolic function has detrimental effects on ventricular performance, since mechanical work is wasted stretching some regions at the expense of stroke volume [22]. Possible mechanisms for functional heterogeneity include regional variations in afterload (wall stress), impaired relaxation, decreased contractile efficiency and perfusion defects [22]. These are briefly considered below.

4.2. Possible mechanisms of regional heterogeneity

The degree of myocardial shortening has been shown to be strongly correlated with geometric measures of wall stress and the relationship between ES wall stress and shortening is commonly used to provide a measure of LV performance independent of afterload [17]. In DCM patients, Hayashida et al. [3] found a strong negative correlation between regional GS (Janz formula) and regional EF measured using left ventriculography. Fujita et al. [4] noted a similar regional relationship from apex to base using cine MRI. In the present study, regional shortening did appear to reduce with increased regional GS. However, GS could not explain the regional differences in shortening around the ventricle. Although similar formulae are frequently used to estimate global stress [17], Eq. (2) is unlikely to provide realistic estimates of regional wall stress, since it takes no account of the non-linear anisotropic material properties of myocardium [18,19]. Using a finite element model of the systolic heart, Costa [19] found that the Mirsky thick-walled ellipsoid model provided the best correlation with true stress of several geometrically-based stress formulae, but the correlation was weak ($r^2 = 0.07$) and errors were relatively large (100–200%). However, GS is an index that incorporates pressure and the major geometric determinants of stress (curvature and wall thickness) and therefore may be useful for the purposes of comparing regional geometry between and within patients.

Bach et al. [1] measured regional oxidative metabolism in non-ischemic DCM patients by carbon-11 acetate clearance kinetics on dynamic positron emission tomography. Regional oxidative metabolism was positively correlated with regional function, as measured using 2D echocardiography. The proximal lateral wall was most likely to have preserved function and this region was associated with the greatest oxidative metabolism. Our results also showed greatest shortening (and therefore greatest mean velocity of shortening) in the lateral wall. This is consistent with greater oxidative metabolism in this region since oxidative metabolism is known to be dependent on shortening velocity. Interestingly, Yokoyama et al. [27] found that homogeneous myocardial glucose utilization rate (coefficient of variation $<13.6\%$) can predict both prognosis and improvement of LV function by medical therapy in DCM patients.

Regional variations in myocardial perfusion have also been described in non-ischemic DCM patients [5,28,29]. Using qualitative assessment of thallium-201 tomograms, Jullière et al. [5] found that reduced uptake was more common in anterior, inferior and apical regions than in septal and lateral segments. van den Heuvel et al. [28] used positron emission tomography to evaluate regional ischemia in 22 idiopathic DCM patients, finding reduced myocardial blood flow (MBF) reserve which was correlated with wall stress. Mismatch between flow and glucose

metabolism occurred in regions of low MBF reserve and these regions were also associated with a switch from aerobic to anaerobic metabolism. Although these findings indicate the presence of regional hibernation or chronic ischemia, regional patterns of reduced MBF or mismatch were not reported. Parodi et al. [29] observed reduced myocardial blood flow in DCM patients with ^{99m}Tc labeled microspheres injected during heart transplant, but no significant regional differences were found. Some fibrosis was observed histologically, especially in the subendocardial layer, but this did not correlate with blood flow. Heterogeneity of flow and function may be also accompanied by heterogeneous alterations in expression of β-adrenergic receptors [30], natriuretic peptides [31], SERCA2a mRNA and protein, and phospholamban [32].

4.3. Recovery of function after PLV

The post-PLV results show that, at least in some subjects, it is possible for septal, anterior and posterior function to improve toward more normal values with surgical intervention. This indicates a potential for improvement of regional function with therapy. The mechanism for functional improvement with PLV is not clear, but is thought to be due to normalization of wall stress [12,33]. Popovic et al. [33] studied 19 patients pre- and post-PLV with echocardiography and found that ejection fraction improved with reduction of wall stress along lines parallel to the normal stress-shortening relationship. Similarly, Fig. 5 shows that regional shortening improved with stress normalization in all regions except the site of surgical reapproximation of the LV free wall. Septal dysfunction in nonischemic DCM may therefore be (at least partly) due to increased regional afterload and not to an irrecoverable loss of contractility. Despite the loss of contractility in the lateral wall, our results show a reduction in regional heterogeneity post-PLV. This may in itself have beneficial effects on ventricular function [22], since more of the work done is translated to pump function.

4.4. Limitations and further study

In this study only five patients could be investigated both before and after PLV. A significant percentage of DCM patients had unsatisfactory outcome from PLV [12] and many patients required ICD, pacemaker or required support from an assist device. Therefore, most patients were not suitable for post-PLV assessment of LV mechanics by MR tagging. In addition, all patients in this study had mitral valve repair, including a annuloplasty ring and Alfieri repair, the influence of which on regional function is not known. However, the fact that all five patients imaged after PLV showed substantial improvement in septal function implies that the regional dysfunction is, to some extent, recoverable.

The temporal characteristics of regional shortening were not investigated in this study. Early septal contraction could be identified in some patients in the first frame of the cine sequence; however, it was felt that the temporal resolution of the images was insufficient to accurately quantify regional differences in onset of contraction.

Acknowledgements

We are grateful for the support of the Health Research Council of New Zealand (96/164) and the Cleveland Clinic Foundation. We thank Drs. C.M. Kramer, V.A. Ferrari, N. Reichek and L. Axel for the use of the normal data analyzed in this study.

Appendix A. Strain measurements

As described previously [11], the deformation gradient tensor F was calculated directly from the finite element model. Tensor components were referred to a locally Cartesian body coordinate system aligned in the circumferential (C), longitudinal (L) and radial (R) directions. Green's strain tensor, referred to the CLR system, is defined as

$$E = \frac{1}{2}(F^{\mathrm{T}}F - I) \tag{A1}$$

Components of E were reported in [11] for 12 normal volunteers. Percentage shortening (defined in Eq. (1)) in each of the C, L and R directions were calculated from E using

$$\%S_{\mathrm{A}} = \left(1 - \sqrt{1 + 2E_{\mathrm{AA}}}\right) \cdot 100\% \tag{A2}$$

[14], where A is one of the C, L or R directions, $\%S_{\mathrm{A}}$ is the percentage shortening or lengthening and E_{AA} is the corresponding component of the strain tensor. Shear angles were calculated from E using

$$\sin \alpha_{\mathrm{AB}} = \frac{2E_{\mathrm{AB}}}{\sqrt{1 + 2E_{\mathrm{AA}}}\sqrt{1 + 2E_{\mathrm{BB}}}} \tag{A3}$$

where A and B are one of the C, L or R directions (not both the same), α_{AB} is the change in angle between infinitesimal line segments initially oriented at right angles in the A and B directions and E_{AB}, E_{AA} and E_{BB} are corresponding components of the Green strain tensor [14]. Principal strains [11] may be calculated as the eigenvalues of E, these may also be converted to principal shortening values using Eq. (A2).

References

[1] Bach DS, Beanlands RS, Schwaiger M et al. Heterogeneity of ventricular function and myocardial oxidative metabolism in nonis-

chemic dilated cardiomyopathy. J Am Coll Cardiol 1995;25:1258–1262.

[2] Uematsu M, Miyatake K, Tanaka N et al. Myocardial velocity gradient as a new indicator of regional left ventricular contraction: detection by a two-dimensional tissue Doppler imaging technique. J Am Coll Cardiol 1995;26:217–223.

[3] Hayashida W, Kumada T, Nohara R et al. Left ventricular regional wall stress in dilated cardiomyopathy. Circulation 1990;82:2075–2083.

[4] Fujita N, Duerinckx AJ, Higgins CB. Variation in left ventricular regional wall stress with cine magnetic resonance imaging: normal subjects versus dilated cardiomyopathy. Am Heart J 1993;125:1337–1345.

[5] Juillière Y, Marie PY, Danchin N et al. Radionuclide assessment of regional differences in left ventricular wall motion and myocardial perfusion in idiopathic dilated cardiomyopathy. Eur Heart J 1993;14:1163–1169.

[6] Axel L, Dougherty L. Heart Wall motion: Improved method of spatial modulation of magnetization for MR imaging. Radiology 1989;172:349–350.

[7] Young AA, Axel L, Dougherty L et al. Validation of tagging with MRI to estimate material deformation. Radiology 1993;188:101–108.

[8] Young AA, Imai H, Chang C-N et al. Two-dimensional left ventricle motion during systole using MRI with SPAMM. Circulation 1993;89:740–752.

[9] Palmon LC, Reichek N, Yeon SB et al. Intramural myocardial shortening in hypertensive left ventricular hypertrophy with normal pump function. Circulation 1994;89:122–131.

[10] Young AA, Kraitchman DL, Dougherty L et al. Tracking and finite element analysis of stripe deformation in magnetic resonance tagging. IEEE Trans Med Imag 1995;14:413–421.

[11] Young A.A., Kramer C.M., Ferrari V.A., Axel L., Reichek N. Three-dimensional left ventricular deformation in hypertrophic cardiomyopathy. Circulation 1994;90:854–867. 1995;14:413–421.

[12] McCarthy PM, Starling RC, Wong J et al. Early results with partial left ventriculectomy. J Thor Cardiovasc Surg 1997;114:755–765.

[13] Hunter PJ, Smaill BH. The analysis of cardiac function: A continuum approach. Prog Biophys molec Biol 1988;52:101–164.

[14] Fung YC. Foundations of solid mechanics, Englewood Cliffs, NJ: Prentice-Hall, 1965.

[15] Mirsky I. Elastic properties of myocardium: A quantitative approach with physiological and clinical applications. In: Berne RM, editor, Handbook of physiology, Vol. 2, Washington, DC: American Physiological Society, 1979, pp. 497–531.

[16] Young AA, Orr R, Smaill BH et al. Three-dimensional changes in left and right ventricular geometry in chronic mitral regurgitation. Am J Physiol: Heart Circ Physiol 1996;271:H2689–H2700.

[17] Borow KM, Green LH, Grossman W et al. Left ventricular end-systolic stress–shortening and stress–length relations in humans: Normal values and sensitivity to inotropic state. Am J Cardiol 1982;50:1301–1308.

[18] Yin FCP. Ventricular wall stress. Circ Res 1981;49:829–842.

[19] Costa KD. The structural basis of three-dimensional ventricular mechanics. University of California San Diego, 1996, Chapter 4. Thesis.

[20] Schiller NB, Shah PM, Crawford M et al. Recommendations for quantification of the left ventricle by two-dimensional echocardiography. J Am Soc Echo 1989;2:358–367.

[21] Ingels NB, Hansen DE, Daughters GT et al. Relation between longitudinal, circumferential, and oblique shortening and torsional deformation in the left ventricle of the transplanted human heart. Circ Res 1989;64:915–927.

[22] Lew WYW. Functional consequences of regional heterogeneity in the left ventricle. In: Glass L, Hunter P, McCulloch A, editors, Theory of heart: biomechanics, biophysics and nonlinear dynamics of cardiac function, New York: Springer-Verlag, 1991, pp. 209–237.

[23] van Rugge FP, Holman ER, van der Wall EE et al. Quantitation of global and regional left ventricular function by cine magnetic resonance imaging during dobutamine stress in normal human subjects. Eur Heart J 1993;14:456–463.

[24] Borges AC, Pingitore A, Cordovil A et al. Hetrogeneity of left ventricular regional wall thickening following dobutamine infusion in normal human subjects. Eur Heart J 1995;16:1726–1730.

[25] Sunnerhagen KS, Bhargava V, Shabetai R. Regional left ventricular wall motion abnormalities in idiopathic dilated cardiomyopathy. Am J Cardiol 1990;65:364–370.

[26] MacGowan GA, Shapiro EP, Azhari H et al. Noninvasive measurement of shortening in the fiber and cross-fiber directions in the normal human left ventricle and in idiopathic dilated cardiomyopathy. Circulation 1997;96:535–541.

[27] Yokoyama I, Momomura S, Ohtake T et al. Role of positron emission tomography using fluorine-18 fluoro-2-deoxyglucose in predicting improvement in left ventricular function in patients with idiopathic dilated cardiomyopathy. Eur J Nucl Med 1998;25:736–743.

[28] van den Heuval AFM, van Veldhuisen DJ, van der Wall EE et al. Regional myocardial blood flow reserve impairment and metabolic changes suggesting myocardial ischemia in patients with idiopathic dilated cardiomyopathy. J Am Coll Cardiol 2000;35:19–28.

[29] Parodi O, De Maria R, Oltrona L et al. Myocardial blood flow distribution in patients with ischemic heart disease or dilated cardiomyopathy undergoing heart transplantation. Circulation 1993;88:509–522.

[30] Simmons WW, Freeman MR, Grima EA et al. Abnormalities of cardiac sympathetic function in pacing-induced heart failure as assessed by [^{123}I]metaiodobenzylguanidine scintigraphy. Circulation 1994;89:2843–2851.

[31] Tanaka M, Hiroe M, Nishikawa T et al. Cellular localization and structural characterization of natriuretic peptide-expressing ventricular myocytes from patients with dilated cardiomyopathy. J Histochem Cytochem 1994;42:1207–1214.

[32] Prestle J, Dieterich S, Preuss M et al. Transmural differences in expression of calcium handling proteins and atrial natriuretic factor in end-stage failing human myocardium (abstract). Circulation 1997;96:I–118.

[33] Popovic Z, Miric M, Gradinac S et al. Effects of partial left ventriculectomy on left ventricular performance in patients with nonischemic dilated cardiomyopathy. J Am Coll Cardiol 1998;32:1801–1808.